MATERIALS SCIENCE

Assignment of enantiomorphs for the chiral allotrope β-Mn by diffraction methods

Ulrich Burkhardt[1]*, Aimo Winkelmann[2]*, Horst Borrmann[1†], Andreea Dumitriu[1†], Markus König[1†], Grzegorz Cios[2†], Yuri Grin[1]*

The assignment of enantiomorphs by diffraction methods shows fundamental differences for x-rays and electrons. This is particularly evident for the chiral allotrope of β-Mn. While it is not possible to determine the sense of chirality of β-Mn with established x-ray diffraction methods, Kikuchi pattern simulation of the enantiomorphs reveals differences, if dynamical electron diffraction is considered. Quantitative comparison between experimental and simulated Kikuchi patterns allows the spatially resolved assignment of the enantiomorph in polycrystalline materials of β-Mn, as well as the structurally strongly related phase Pt_2Cu_3B. On the basis of enantiomorph distribution maps, crystals were extracted from enantiopure domains by micropreparation techniques. The x-ray diffraction analyses confirm the assignment of the Kikuchi pattern evaluations for Pt_2Cu_3B and do not allow to distinguish between the enantiomorphs of β-Mn.

INTRODUCTION

All chiral crystal structures belong to the Sohncke space groups, which contain only symmetry elements of the first kind, i.e., rotations, rototranslations, and translations, but no inversion centers, rotoinversion axes, or mirror planes, e.g., symmetry elements of the second kind (*1*, *2*). Among the Sohncke groups, there are 11 pairs of space groups that are chiral (*1*), i.e., the symmetry element arrangements can be understood as mirror or inversion images of each other. Two of them—$P4_132$ and $P4_332$—are in focus of the present study. The symmetry restriction in chiral crystal structures has far-reaching consequences both for the material properties and for the approaches suitable to distinguish between the two enantiomorphs. Certain material properties, such as optical birefringence, only occur in phases with chiral crystal structure, but also unusual ordered, electronic states such as noncollinear spin structures (*3*), or the occurrence of unconventional superconductivity (*4*) is closely related to the chirality of the underlying material. Despite such often close structure-property relationships, the experimental determination or assignment of the absolute structure is challenging. The presence of both enantiomorphs in a material may lead to a weakening or even complete extinction of a chirality-dependent property. The assignment of the sense of chirality—or "fixing the enantiomorph" (*1*)—with good spatial resolution in polycrystalline materials is fundamental in the experimental investigation of chirality-related properties (*5*, *6*). The determination of the absolute structure is possible by x-ray diffraction or—in the case of electrons—with the convergent beam electron diffraction method. In both cases above, additional scattering contributions occur, which lead to different structure factors in Bijvoet pairs. In x-ray single-crystal diffraction, the contribution of the anomalous dispersion leads to an element-specific and wavelength-dependent phase shift of the scattered wave (*7*, *8*). This does not work if the crystal contains only one type of atoms showing the same anomalous dispersion effect (*8*, *9*). In electron diffraction, however, it is the influence of multiple scattering processes that leads to a deviation from the kinematic scattering and allows the assignment of the enantiomorphs (*10*–*12*).

In addition to the well-established methods for the assignment of the absolute structure—x-ray diffraction and transmission electron microscopy—the electron backscatter diffraction (EBSD) technique has been established in recent years, which allows spatially resolved analysis of grain orientation in a scanning electron microscope (SEM) (*13*). With EBSD, it is possible to crystallographically characterize the surface of millimeter-sized polycrystalline materials with a spatial resolution down to 40 nm (*14*). EBSD is mainly based on the measurement and evaluation of Kikuchi patterns, which result from electron diffraction. However, experimental Kikuchi patterns are also sensitive to the absolute structure where the assignment of the enantiomorph was confirmed by morphological characterization in the case of α-quartz (*15*) or x-ray single-crystal investigations in the case of the intermetallic phase CoSi (*16*). Recent progress in the understanding of electron scattering processes in Kikuchi pattern formation allows their simulation in a very detailed way. In particular, the dynamical scattering processes lead to accurate reproduction of the differences in the experimental patterns of enantiomorphs (*17*). The local assignment of the sense of chirality can therefore be done by comparing an experimental Kikuchi pattern with the simulation for both enantiomorphs. As a result, maps can be created, which show the distribution of the enantiomorphs in the polycrystalline material (*18*). The local sense of chirality becomes an easily accessible property of polycrystalline materials. In the present work, we use the new approach to identify enantiomorphs of β-Mn and the structurally related phase Pt_2Cu_3B.

β-Mn is one of the rather rare examples of a chiral allotrope where atoms differ in local environment. β-Mn is a high-temperature phase that is stable in the range 727°C < T < 1100°C. The limited temperature stability range and the high vapor pressure of Mn at elevated temperatures are major factors that make it difficult to prepare single crystals of this phase especially with defined sense of chirality. The crystal structure was determined from single-crystal x-ray data using single crystalline specimen of irregular shape obtained by fragmentation samples annealed at 850°C before quenching

[1]Max-Planck-Institut für Chemische Physik fester Stoffe, 01187 Dresden, Germany. [2]Academic Centre for Materials and Nanotechnology, AGH University of Science and Technology, 30-059 Kraków, Poland.
*Corresponding author. Email: ulrich.burkhardt@cpfs.mpg.de (U.B.); winkelmann@agh.edu.pl (A.W.); grin@cpfs.mpg.de (Y.G.)
†These authors contributed equally to this work.

(*19*, *20*). Within a cubic unit cell (space group $P4_132$), two positions are occupied, Mn1 at 12*d* $(\frac{1}{8}, y, y+\frac{1}{4})$ and Mn2 at 8*c* (*x*, *x*, *x*). While the eightfold position has an icosahedral coordination, in the case of the 12*d* position, two more atoms belong to the coordination polyhedron [coordination number (CN) = 14]. A remarkable symmetry property of the crystal structure is the arrangement of nonintersecting screw axes parallel to the <1 0 0> directions. The two enantiomorphs differ in the screw direction of the axes and show exclusively 4_1 or 4_3 screw axes (Fig. 1, top). An important feature is the strong anisotropy of atomic displacement parameters for the 12*d* position. However, the sense of chirality could not be determined. The special crystal chemical aspects of the structure were discussed in detail (*21*, *22*). The differences between the Mn atoms in coordination and anisotropy of atomic displacement and also the reported different contributions of the atoms on Mn1 and Mn2 positions to the magnetism of the phase (*23*) are strong indications that the Mn atoms show different crystal chemical behaviors. Because of the missing (or at least small) differences in the anomalous scattering contribution, it is accepted that in general experiments x-ray diffraction data are not sensitive to the sense of chirality of the structure of elements (*9*). However, sensitivity may occur if direction-dependent scattering contributions play a substantial role (*9*, *24*, *25*).

β-Mn is particularly suitable for this investigation because several multicomponent isotypes or closely related crystal structures exist, allowing the determination of the absolute structure from single-crystal x-ray diffraction data. Here, we have chosen the ternary phase Pt_2Cu_3B (*26*). The symmetry is described by the same space groups as the two enantiomorphs of β-Mn. In Pt_2Cu_3B, the 12*d* position is mixed occupied by Pt/Cu, whereas the 8*c* position is exclusively occupied by Cu. Boron is located at the interstitial site 4*a* (Fig. 1, bottom). The occupancy of the atom positions 12d and 8c by different elements allows to assign the enantiomorph by x-ray diffraction. Pt_2Cu_3B is a superconductor with a transition temperature of about 2.06 K (*26*).

A combination of x-ray diffraction and EBSD analysis previously introduced for the chiral CoSi phase (*16*) is applied to investigate polycrystalline materials of Pt_2Cu_3B and β-Mn. Preliminary EBSD studies on β-Mn are reported in (*27*). First, we present the analyses of the phase Pt_2Cu_3B, where the assignment of the enantiomorphs by the Kikuchi pattern analysis is proven by x-ray single-crystal diffraction experiments. In the next step, the same approach is used to investigate the polycrystalline material of β-Mn.

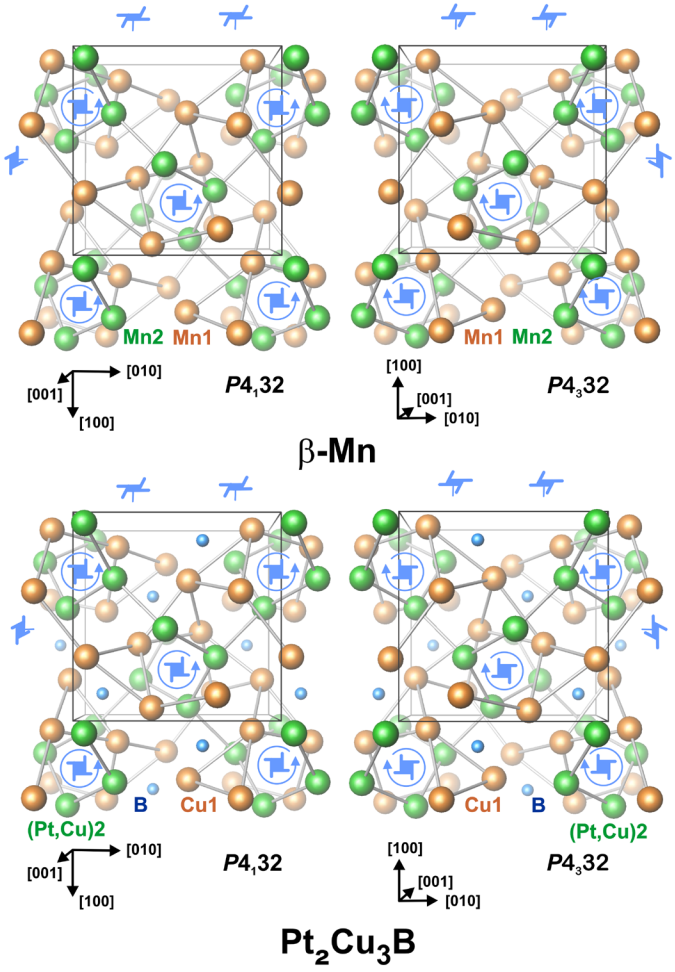

Fig. 1. Crystal structures of enantiomorphs of β-Mn (top) and Pt_2Cu_3B (bottom) (perspective view). Blue squares and circles symbolize screw axes 4_1 (left) and 4_3 (right) perpendicular and parallel (tilted symbols) to the drawing plane.

RESULTS

The assignment of the enantiomorphs for different grains in the polycrystalline materials of Pt_2Cu_3B and β-Mn is carried out by a quantitative comparison of the experimental Kikuchi patterns with simulated ones for both respective enantiomorphs. The basis for this method is the simulation of the Kikuchi pattern using the Bloch wave approach to dynamical electron diffraction, where the implementation of multiple scattering of electrons leads to absolute structure-dependent contributions (*15*). For the assignment of the enantiomorphs from experimental Kikuchi pattern, the better match with one of the two simulated patterns is decisive. Experimental and simulated patterns are compared in a quantitative way by the calculation of the cross-correlation coefficient *r* (*28*). This parameter may vary in the range $0 \leq |r| \leq 1$, e.g., between vanishing ($r = 0$) and complete ($|r| = 1$) matching of patterns. The two enantiomorphs of each of the phases investigated here differ in their space groups, where we specify that the match of the simulated with experimental patterns is given by the cross-correlation coefficients r_+ (experiment versus simulation in $P4_132$) and r_- (experiment versus simulation in $P4_332$). A reliable assignment of the enantiomorph demands large mean value $r_m = {}^1/_2\,(r_+ + r_-)$, i.e., that there has to be a generally good agreement between the experimental and two simulated patterns. In particular, the experimental pattern must be of high quality for a meaningful analysis. Furthermore, the difference $|\Delta r| = |r_+ - r_-|$ between the cross-correlation coefficients must be sufficiently large. This is only fulfilled if there are notable chirality-dependent contributions and consequently substantial differences between the simulated patterns. A measure for the differences between simulated patterns of the two enantiomorphs is the cross-correlation coefficient r_{sim} (simulation in $P4_132$ versus simulation in $P4_332$). In the case that there are no differences between the simulated patterns of the enantiomorphs, it applies that $r_{sim} = 1$. In the Kikuchi pattern analyses presented below, the values are $r_{sim} \approx 0.90$ (Pt_2Cu_3B) and $r_{sim} \approx 0.96$ (β-Mn), which can be considered as sufficiently large for experimental observation. Reliable assignment of the enantiomorphs

from experimental Kikuchi patterns by the cross-correlation method are realized for $|\Delta r| \geq 0.01$ at $r_m \geq 0.5$ in previous investigations under similar measurement conditions (*16*, *18*).

The investigation of the Pt_2Cu_3B phase is performed on metallographically prepared polycrystalline material. Several grains of this phase are shown in the SEM-based orientation contrast image resulting from the evaluation of the total intensities of the EBSD detector signal (Fig. 2, top left). Small grains of the minority phase PtCu are situated at the grain boundaries of the majority Pt_2Cu_3B. Well-established methods of Kikuchi pattern analysis are applied to identify the two phases. Both phases have been verified by x-ray powder diffraction. The cross-correlation analysis of the experimental EBSD pattern reveals values of $r_m \geq 0.55$ (Fig. 2, middle left) and $|\Delta r| \geq 0.01$ (Fig. 2, bottom left) so that—with the exception of the grain boundaries and grains of the PtCu minority phase—the absolute structure was assigned to each single Kikuchi pattern of the experimental EBSD area mapping. The pattern simulation shows that the Kikuchi patterns of the two enantiomorphs are very similar (Fig. 3, first row). This is generally true for the complete diffraction sphere and is shown for two grains with different orientations in Fig. 3. The pattern evaluation assigns different enantiomorphs to these grains by the quantified comparison between experimental and simulated patterns. For each grain orientation, it applies that the differences in the simulated patterns occur in most areas of the patterns (Fig. 3, second row right) while maintaining the general diffraction motif. This leads to different cross-correlation coefficients, which in the case of grain 1 (Fig. 3, first and second rows) amounts to $\Delta r = r_+ - r_- = 0.645 - 0.617 = +0.028$ because of the better match with the simulation of the enantiomorph $P4_132$. The experimental pattern of grain 2 (Fig. 3, third and fourth rows) matches more the simulation of the $P4_332$ enantiomorph with $\Delta r = r_+ - r_- = 0.600 - 0.630 = -0.030$. The calculation of the cross-correlation coefficients takes all differences between experimental and simulated patterns into account and is the basis for the assignment of the enantiomorphs. In addition, a visual inspection of local features of the Kikuchi pattern also indicates the assignment of the enantiomorphs.

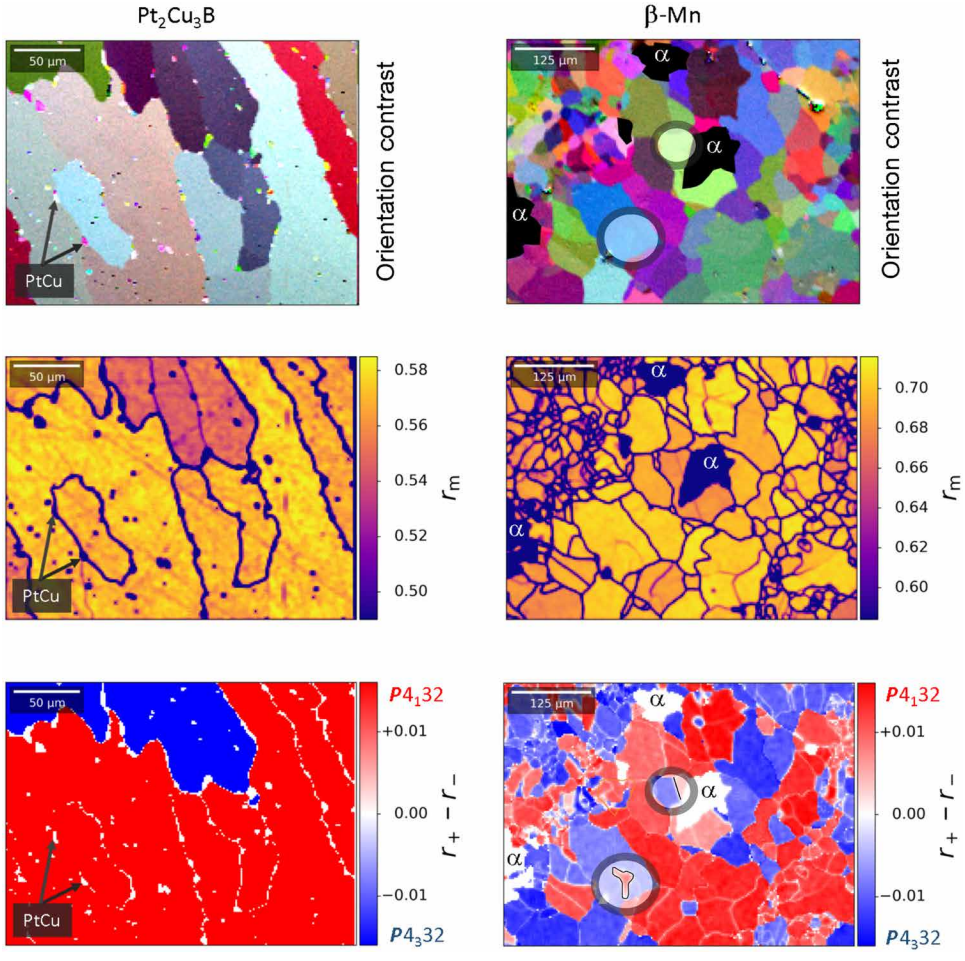

Fig. 2. Spatially resolved assignment of the absolute structure in polycrystalline materials. Left column: Grains of Pt_2Cu_3B and the minority phase PtCu mainly situated at grain boundaries of the majority phase. Right column: Grains of β-Mn and the minority phase α-Mn. Top row: Grains of the respective majority phase. Grain orientation is given qualitatively. The contrast is based on the differential backscattered electron signal from various regions of the EBSD detector; PtCu grains are represented by colored dots; α-Mn grains are black. Middle row: Color-coded maps of the average normalized cross-correlation coefficient $r_m = {}^1/_2 (r_+ + r_-)$; grain boundaries and the minority phase PtCu or α-Mn are black ($r_m << 0.5$). Bottom row: Enantiomorph distribution maps; color-coded maps show the normalized cross-correlation coefficient difference, $\Delta r = r_+ - r_-$; grain boundaries and the minority phase PtCu or α-Mn are white ($\Delta r \approx 0$). Highlighted circles (right) contain boundaries (black) between different enantiomorphs of β-Mn, which are not related to large angle grain boundaries. Respective areas of the grain orientation map (top right) look homogeneous.

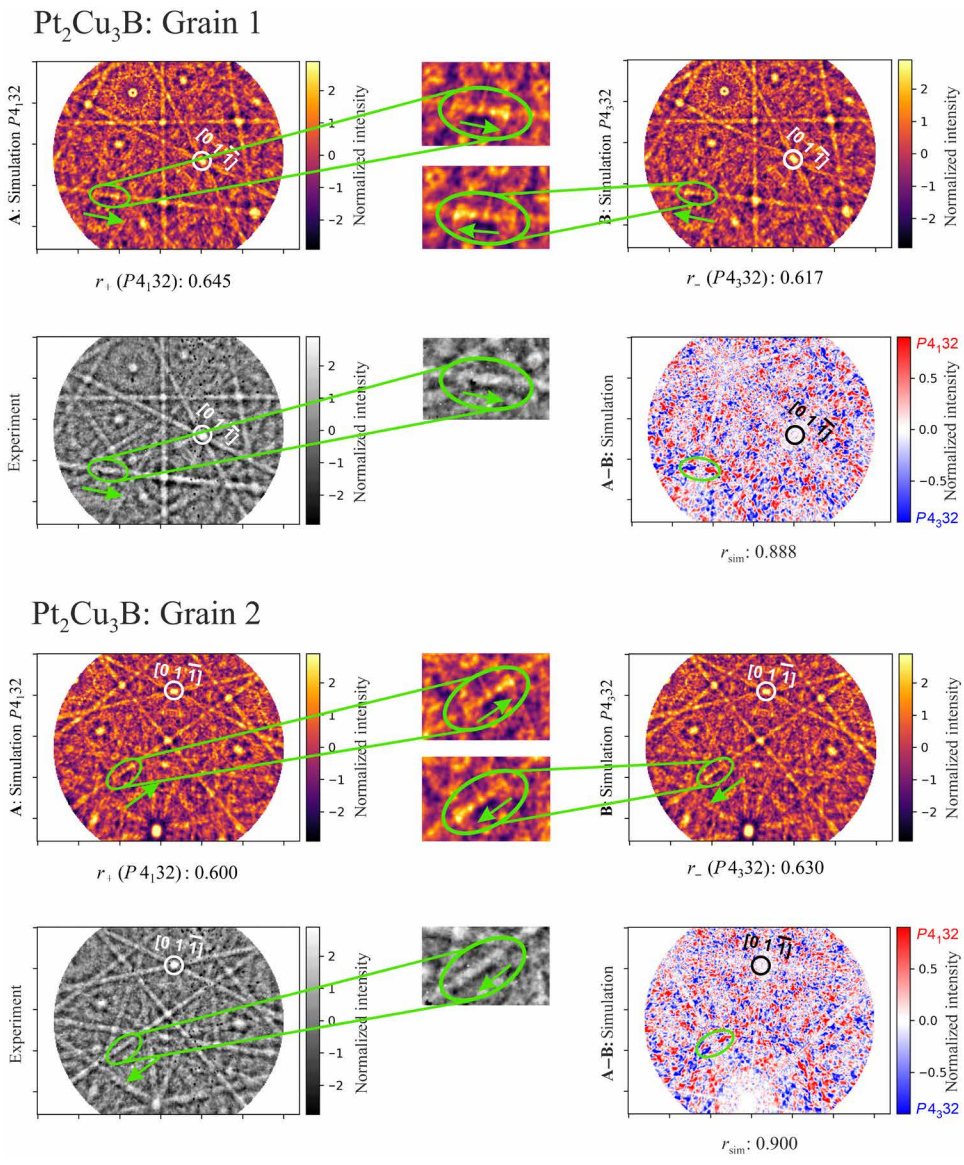

Fig. 3. Assignment of the absolute structure of Pt_2Cu_3B from single Kikuchi pattern. Gnomonic projection of Kikuchi patterns of grain 1 (first and second rows) and grain 2 (third and fourth rows) of the polycrystalline material Pt_2Cu_3B with different grain orientation and different absolute structure. The poles [01$\bar{1}$] are shown for guidance. Simulated and experimental pattern intensities are normalized to zero mean and unit SD; acceleration voltage, 30 kV. First and third rows: Simulated Kikuchi patterns for the enantiomorphs A ($P4_132$) (left) and B ($P4_332$) (right); the very similar patterns show specific local features (detail enlargement, middle). Green circles mark neighbored, intensive spots; arrows point to higher intensity; the cross-correlation coefficients $r_+(P4_132)$, $r_-(P4_332)$ quantify the match between the experimental and respective simulated Kikuchi pattern. Second and fourth rows: (Left) Experimental Kikuchi patterns. The intensity distribution of the local pattern motif (green circle) can be assigned to one of the two simulated patterns (parallel arrows). (Right) Intensity differences between the simulated patterns; regions with equal intensities (A = B) are white; the cross-correlation coefficients r_{sim} quantify the match between the simulated patterns A and B.

Here, as mentioned before for the whole patterns, the local motif is the same for the two simulated patterns, but they differ in the intensity distribution. Detail enlargements of the patterns in Fig. 3 (middle column) visualize neighboring spots, where the intensity distributions are different in the two simulated patterns. Comparing the respective intensity distribution of the experimental pattern of grain 1 indicates a better match with the simulation of the enantiomorph $P4_132$. The same analysis for grain 2 shows a better match with the simulated pattern of the enantiomorph $P4_332$. Both assignments are in accord with the cross-correlation method. The evaluation of each Kikuchi pattern of the EBSD area mapping results in an enantiomorph distribution map with high spatial resolution for the complete polycrystalline material (Fig. 2, bottom left). Grain boundaries, which are also shown in the SEM-based orientation map (Fig. 2, top left), are well reproduced. An assignment of the enantiomorph along grain boundaries is not possible because of the reduced pattern quality in these regions, e.g., the two cross-correlation coefficients r_+ and r_- are small and do not differ substantially. The same applies to the areas of the minority phase PtCu, but here, the small values of r_+, r_- result from the poor match of the experimental patterns with

the simulated patterns of the Pt_2Cu_3B phase. Thus, the grain boundaries and minority phase show almost the same r_m values (Fig.2, middle left), and $|\Delta r|$ values are small (Fig. 2, bottom left, and fig. S1). The enantiomorph distribution map reveals a very unbalanced distribution in both the arrangement and area fractions (Fig. 2, bottom left). There are two enantiopure domains in the investigated area with a ratio of approximately 1:5 and larger fraction of the enantiomorph $P4_132$. Investigation of another larger fragment also shows a likewise unbalanced distribution with a ratio of 20:1 and a strong preference for the $P4_332$ enantiomorph (fig. S2).

Using the enantiomorph distribution maps of the two fragments, one crystal of each enantiomorph was cut from enantiopure areas using a focused ion beam (FIB) technique. The positions of the two crystals in the polycrystalline material and the relation to the respective enantiomorph distribution maps are given in figs. S1 and S2, respectively. Crystal 1 was taken from a grain assigned to the enantiomorph with space group $P4_132$. The structure refinement in this space group confirms the previously obtained crystal structure (*20*) and yields a Flack parameter of $x = -0.02(1)$. Crystal 2 was cut from a grain assigned to the enantiomorph with space group $P4_332$. The structure refinement in this space group reveals the Flack parameter of $x = -0.01(1)$. Thus, the single-crystal x-ray diffraction experiments confirm the assignment of the enantiomorph from Kikuchi pattern analysis. Detailed information on the crystal structure refinements from x-ray diffraction data is collected in Table 1. Significant differences between the structure factors F of Bijvoet pairs with respect to their experimental accuracy σ show reflections (1 2 3)/(−1 −2 −3) and (1 2 4)/(−1 −2 −4) with values $|\Delta F^2|/\sigma = 2.6$ and $|\Delta F^2|/\sigma = 2.0$, respectively. Several other Bijvoet pairs show $|\Delta F^2|/\sigma$ values close to 2. Within the accuracy of the measurement, these values are the same for the two crystals of Pt_2Cu_3B, but the differences between the structure factors change sign when the absolute structure changes. The identical assignment of the enantiomorphs from x-ray diffraction and EBSD data shows the consistency and reliability of the results obtained from the differences in the cross-correlation coefficients.

The procedure described above for Pt_2Cu_3B was applied in an identical way to the β-Mn phase. The investigations were carried out on a metallographically prepared polycrystalline material that contains grains of the majority phase β-Mn and small amount of the minority phase α-Mn. Grain size and shape of the phases α-Mn and β-Mn are almost the same, but well-established EBSD pattern analysis reveals a clear phase identification (Fig. 2, top right, and figs. S3, top left, and S4). The evaluation of the EBSD pattern using the cross-correlation method results in values of $r_m \geq 0.65$ (Fig. 2, middle right) and $|\Delta r| \approx 0.01$ (Fig. 2, bottom right). These values reflect the good match between the experimental and simulated patterns and indicate the high quality of the experimental patterns. The differences between the cross-correlation coefficients r_+ and r_- are sufficient to identify the better match of the experimental and one of the two simulated patterns. Thus, an assignment of the enantiomorphs by the cross-correlation method is possible. The patterns of two grains of β-Mn with a different orientation and also a different sense of chirality are shown in Fig. 4. Keeping the different grain orientation in mind, the diffraction patterns of Pt_2Cu_3B (Fig. 3) and β-Mn (Fig. 4) show many similarities. The most considerable differences exist in the intensities of the Kikuchi lines and zone axes. This reflects the close relation between the crystal structures of β-Mn and Pt_2Cu_3B showing the same symmetry and chemically different occupancy of the atom positions 12*d* and 8*c*. Nevertheless, the differences in the simulated pattern of both enantiomorphs related to grain 1 (Fig. 4, second row right) and grain 2 (Fig. 4, fourth row right) of β-Mn are comparable to simulated patterns of Pt_2Cu_3B discussed above. As with Pt_2Cu_3B, the pattern simulations for the β-Mn enantiomorphs show the same motif with intensity variations in many regions. For β-Mn grain 1, the cross-correlation method gives $\Delta r = r_+ - r_- = 0.713 - 0.723 = -0.010$ with a better match to the simulation of the enantiomorph $P4_332$. For grain 2, the analysis results in $\Delta r = r_+ - r_- = 0.737 - 0.720 = +0.017$ because of the better match with the simulation of the enantiomorph $P4_132$. Also, comparing local intensity distributions in characteristic regions of the EBSD patterns reveals differences between the simulated pattern of β-Mn (Fig. 4, middle column) that are comparable to the behavior described for Pt_2Cu_3B. In the case of β-Mn grain 1, the analysis of the intensity distribution of a selected local pattern motif indicates the better match of the experimental pattern with the simulated pattern $P4_332$, and for the experimental pattern of β-Mn grain 2, the simulation $P4_132$ matches better. Thus, the assignment of the enantiomorph for β-Mn is comparable to the Kikuchi pattern analysis for Pt_2Cu_3B in respect to the calculation of the cross-correlation coefficient and also comparing local intensity distributions of experimental and simulated patterns. Applying the cross-correlation method to the patterns of the EBSD area measurement results in the enantiomorph distribution map for the polycrystalline material of β-Mn (Fig. 2, bottom right). Grain boundaries are recovered, and the further comparison with the SEM-based grain orientation map (Fig. 2, top right) reveals that changes of the sense of chirality are related almost exclusively to grain boundaries. Nevertheless, a few boundaries between different enantiomorphs exist (highlights in Fig. 2, bottom right), which apparently are not related to large angle grain boundaries, e.g., within homogeneous areas in the grain orientation map. The investigated polycrystalline material of β-Mn shows approximately the same area fraction for both enantiomorphs. The comparison of the polycrystalline materials β-Mn and Pt_2Cu_3B indicates clear differences in the distribution of the enantiomorphs with a more random distribution for β-Mn and only a few large domains in Pt_2Cu_3B (Fig. 2, bottom left, and fig. S2, middle).

The enantiomorph distribution map was used to identify enantiopure domains suitable for a single-crystal preparation using the FIB technique. Crystals 1 and 2 were cut from domains of the enantiomorph $P4_332$ and $P4_132$, respectively. Details of the crystal positions in the polycrystalline material and the enantiomorph distribution map are shown in fig. S3. Most important information on the single-crystal x-ray diffraction experiments and crystal structure data are given in Table 2. Both β-Mn crystals provided good x-ray diffraction patterns. The structure refinements confirmed the previously obtained structure model for both crystals (*26*). In particular, the large atomic displacement parameters of the 12*d* position are reproduced. However, the enantiomorph cannot be fixed from the x-ray diffraction data. The structure factors of Bijvoet pairs do not differ ($|\Delta F^2|/\sigma \approx 0$) in any of the two datasets. The statistical evaluation provides unphysical values of the Flack parameter in the order of 10^4. The assignment of the absolute structure is therefore impossible (*29*). The small residual values (Table 2) for the crystal structure refinement prove the high quality of the two β-Mn crystals obtained by the FIB preparation technique. The same applies to the two crystals of Pt_2Cu_3B (Table 1). Both findings reveal that crystal quality does not diminish noticeably due to FIB processing. The

Table 1. Crystallographic information of Pt_2Cu_3B crystals.

	Crystal 1		Crystal 2	
Diffraction material	Single crystal		Single crystal	
Crystal shape	Cubic		Cubic	
Crystal size (mm^3)	$0.03 \times 0.03 \times 0.03$		$0.03 \times 0.03 \times 0.03$	
Diffraction system	Rigaku AFC-7		Rigaku AFC-7	
Radiation, wavelength (Å)	MoKα, 0.71073		MoKα, 0.71073	
$\sin\theta/\lambda_{max}$	0.787		0.787	
Unit cell parameter (Å)	6.6666(3)		6.6674(3)	
Unit cell volume ($Å^3$)	296.29(2)		296.39(2)	
Calculated density ($g\ cm^{-3}$)	13.29		13.29	
Ranges in *h*, *k*, *l*	$-9 \le h \le 9$		$-10 \le h \le 10$	
	$-10 \le k \le 10$		$-10 \le k \le 10$	
	$-10 \le l \le 10$		$-9 \le l \le 5$	
Absorption correction	Multiscan		Multiscan	
Absorption coefficient (mm^{-1})	115.30		115.30	
N(hkl) measured	5800		3153	
N(hkl) independent, observed	213, 212		213, 212	
Observation criterion	$F(hkl) \ge 4\sigma(F)$		$F(hkl) \ge 4\sigma(F)$	
Refined parameters	11		11	
Space group	$P4_132$	$P4_332$	$P4_132$	$P4_332$
Atom at Wyckoff site, refined coordinate (*x* or *y*), U_{eq} (in $Å^2$)				
$Pt_{0.67}Cu_{0.33}$ at 12(*d*) $^1/_8, y, y+^1/_4$	0.1919(1)		0.1920(1)	
	0.0127(3)		0.0127(3)	
$Pt_{0.67}Cu_{0.33}$ at 12(*d*) $^1/_8, y, \bar{y}+^1/_4$		0.3080(2)		0.30799(9)
		0.0116(3)		0.0127(2)
Cu at 8(*c*) *x*, *x*, *x*	0.0571(3)	0.9426(4)	0.0571(3)	0.9428(2)
	0.0118(3)	0.0120(5)	0.0118(3)	0.0118(3)
B at 4(*a*) $^3/_8, ^3/_8, ^3/_8$	0.016(7)		0.016(7)	
B at 4(*b*) $^5/_8, ^5/_8, ^5/_8$		0.022(12)		0.016(5)
R_F, *wR*	0.037; 0.041	0.053; 0.056	0.040; 0.043	0.028; 0.031
Flack parameter	−0.02(1)	1.09(8)	1.01(1)	−0.01(1)

x-ray diffraction experiments on the β-Mn crystals also do not show any reflection of the α-Mn phase, which implies stability of the β-Mn phase during FIB treatment.

DISCUSSION

The essential difference between Pt_2Cu_3B and β-Mn structures is the chemically different occupancy of the crystallographic sites 12*d* and 8*c* in Pt_2Cu_3B, while in β-Mn, both are solely occupied by Mn. This different occupancy allows a clear determination of the absolute structure from x-ray single-crystal diffraction data for Pt_2Cu_3B. The chirality sense for β-Mn remained indiscernible by this technique.

The simulation of the Kikuchi patterns shows that dynamical electron diffraction leads to specific changes in the patterns of the respective enantiomorphs of Pt_2Cu_3B and β-Mn. For both phases, these enantiomorph-specific differences are sufficient to assign the absolute structure by the quantified comparison of the experimental Kikuchi pattern with the simulated pattern using the cross-correlation coefficients to quantify the match of experimental and simulated patterns. The reliability of this kind of Kikuchi pattern analysis is confirmed by the x-ray diffraction experiments on Pt_2Cu_3B single crystals that were cut from enantiopure domains of the polycrystalline material. In the case of β-Mn, only the Kikuchi pattern analysis results in the assignment of the enantiomorph applying the same pattern evaluation as for Pt_2Cu_3B. X-ray diffraction experiments

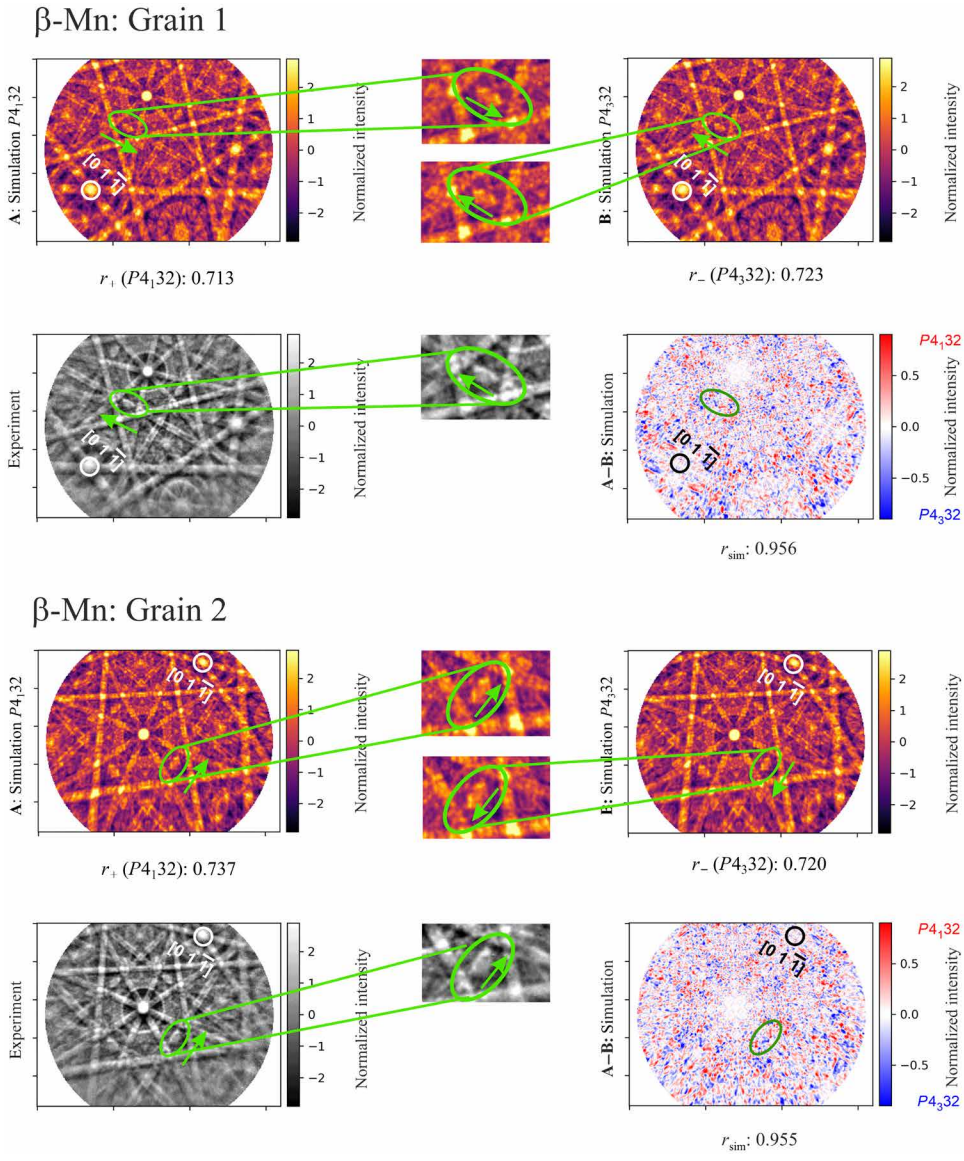

Fig. 4. Assignment of the absolute structure of β-Mn from single Kikuchi pattern. Gnomonic projection of Kikuchi patterns of grain 1 (first and second rows) and grain 2 (third and fourth rows) of polycrystalline β-Mn with different grain orientation and different absolute structure. The poles [01$\bar{1}$] are shown for guidance. Simulated and experimental pattern intensities are normalized to zero mean and unit SD; acceleration voltage, 15 kV. First and third rows: Simulated Kikuchi patterns for the enantiomorphs A ($P4_132$) (left) and B ($P4_332$) (right); the very similar patterns show specific local features (detail enlargement; middle). Green circles mark neighbored, intensive spots; arrows point to higher intensity; the cross-correlation coefficients r_+ ($P4_132$) and r_- ($P4_332$) quantify the match between the experimental and respective simulated Kikuchi patterns. Second and fourth rows: (Left) Experimental Kikuchi patterns. The intensity distribution of the local pattern motif (green circle) can be assigned to one of the two simulated patterns (parallel arrows). (Right) Intensity differences between the simulated patterns; regions with equal intensities (A = B) are white. The cross-correlation coefficients r_{sim} quantify the match between both simulated patterns.

on single crystals of β-Mn with different absolute structure according to the Kikuchi pattern analysis do not reveal any differences in Bijvoet pairs. This analysis shows that the chemical occupancy of the atom sites has different influence on the scattering contributions, causing differences in Bijvoet pairs in x-ray diffraction and electron diffraction–based Kikuchi patterns.

An important part of the presented investigations is the determination of enantiomorph distribution maps for polycrystalline materials from EBSD measurements. This opens various possibilities for systematic studies of porperties depending on the sense of chirality. The enantiomorph distribution map allows to determine overall properties of the polycrystalline material like area fraction of the enantiomorphs as well as their distribution. In addition, the good spatial resolution makes it possible to characterize grain boundaries in respect to changes in the sense of chirality. In combination with the grain orientation map, this can be related to the crystallographic orientations of the participating grains and allows to identify changes in the sense of chirality without noticeable changes in grain orientation. Generally speaking, with the Kikuchi pattern–based method, the sense of chirality is a structural property that can now

Table 2. Crystallographic information for β-Mn crystals.

	Crystal 1		Crystal 2	
Diffraction material	Single-crystal		Single-crystal	
Crystal shape	Cubic		Cubic	
Crystal size (mm^3)	$0.03 \times 0.03 \times 0.03$		$0.03 \times 0.03 \times 0.03$	
Diffraction system	Rigaku AFC-7		Rigaku AFC-7	
Radiation, wavelength (Å)	MoKα, 0.71073		MoKα, 0.71073	
$\sin\theta/\lambda_{max}$	0.760		1.116	
Unit cell parameter (Å)	6.3149(2)		6.3225(2)	
Unit cell volume ($Å^3$)	251.82(1)		252.74(1)	
Calculated density ($g\ cm^{-3}$)	7.24		7.22	
Ranges in *h*, *k*, *l*	$-9 \le h \le 9$		$-14 \le h \le 13$	
	$-9 \le k \le 9$		$-14 \le k \le 14$	
	$-9 \le l \le 8$		$-13 \le l \le 11$	
Absorption correction	Multiscan		Multiscan	
Absorption coefficient (mm^{-1})	23.98		23.90	
N(hkl) measured	2423		11422	
N(hkl) independent, observed	162, 159		499, 162*	
Observation criterion	$F(hkl) \ge 4\sigma(F)$		$F(hkl) \ge 4\sigma(F)$	
Refined parameters	9		9	
Space group	$P4_132$	$P4_332$	$P4_132$	$P4_332$
Atom at Wyckoff site, refined coordinate (*x* or *y*), U_{eq} (in $Å^2$)				
Mn1 at 12(*d*) $^1/_8$, *y*, *y* + $^1/_4$	0.20249(9)		0.20253(6)	
	0.0137(2)		0.0129(2)	
Mn1 at 12(*d*) $^1/_8$, *y*, $\bar{y}$+$^1/_4$		0.29752(9)		0.29747(7)
		0.0137(2)		0.0130(2)
Mn2 at 8(*c*) *x*, *x*, *x*	0.06300(8)	0.93701(8)	0.06292(6)	0.93708(6)
	0.0091(1)	0.0091(1)	0.0078(1)	0.0078(1)
R_F, *wR*	0.022; 0.024	0.022; 0.024	0.017; 0.018	0.017; 0.018
Flack parameter	Nondistinguishable			

*The resolution limit was chosen in agreement with crystal 1 to achieve comparable results.

be related to properties of the polycrystalline material determined with various scanning probe microscopy methods. This also applies to electrically conductive surface layers down to a thickness of approximately 40 nm (*14*).

Furthermore, because of the enantiomorphic distribution map, the concept of ion beam shaping of matter (*30*) can be applied to investigate the dependence of not only bulk but also size-dependent properties on the sense of chirality. FIB machining is used to extract and shape material that is difficult to prepare or where large single crystals are not available. From these studies, it is known that FIB preparation may lead to a thin amorphized surface layer, but bulk properties are unaffected (*30*). This agrees with the single-crystal x-ray diffraction experiments on Pt_2Cu_3B and β-Mn. The Kikuchi pattern analysis before and the x-ray diffraction experiments after the FIB treatment show the same sense of chirality for the crystals of Pt_2Cu_3B. Because of the good quality of the x-ray diffraction patterns, a noticeable influence of the FIB treatment on the bulk material can also be excluded for β-Mn. However, any impact on the sense of chirality of β-Mn cannot be detected with the x-ray diffraction method. Complementary to the present study, it can be considered that recently published machine learning–based algorithms (*31*) allow to determine the crystal symmetry of phases with unknown crystal structure using EBSD data.

MATERIALS AND METHODS

Preparation

The sample preparation of Pt_2Cu_3B was carried out according to the reported procedure (*26*). Polycrystalline samples with a total mass of 1.5 g and nominal composition of $Pt_{33.33}Cu_{50}B_{16.67}$ were prepared

from the elements (Pd: 99.95%, Chempur; Cu: 99.999%, Alfa Aesar; B: 99.99% crystalline, Alfa Aesar) by arc melting. Subsequent heat treatment at 700°C for 43 days, followed by 400°C for 32 days, removed the measurable inhomogeneities of the cast alloy. Phase analysis with energy-dispersive x-ray spectroscopy, well-established EBSD analysis methods, and x-ray powder diffraction techniques showed the majority phase Pt_2Cu_3B and small amounts of the cubic PtCu phase (figs. S1 and S2). The Pt_2Cu_3B phase is stable up to T = 830°C, as thermoanalytical measurements show. The determination of its composition by wavelength-dispersive x-ray spectroscopy on an electron microprobe (Cameca SX100) yielded the composition $Pt_{34.7(2)}Cu_{48.4(2)}B_{16.9\,(1)}$ (atomic %) [$Pt_{67.9(3)}Cu_{30.9(1)}B_{1.83\,(1)}$ (mass %)], which corresponds well to the nominal molar ratio Pt:Cu:B = 2:3:1. Lattice parameter refinement, using the peak positions from the x-ray powder diffraction diagram (fig. S5), yielded a = 6.6577(6) Å. The β-Mn phase was prepared by heating Mn flakes in a sealed quartz ampoule under argon atmosphere. The tube was placed for 5 days at temperature 690°C below the β → α transition point (T = 727°C) and subsequently annealed for 3 days at 850°C. Sufficiently fast quenching of the ampoule in water is necessary to suppress the β → α phase transition. The small portion of the α-Mn detected by well-established EBSD analysis in the polycrystalline material (figs. S3 and S4) is most likely due to kinetic obstacles of the β → α transformation.

EBSD measurement and pattern evaluation

The experimental backscattered Kikuchi diffraction patterns were acquired using an EBSD system (Esprit Vers.2.2; Bruker Nano, Germany) attached to SEM JEOL JSM-7800F. All measured Kikuchi patterns were postprocessed using custom data analysis software (*17*). A best-fit pattern matching approach was used to find the orientation and the sense of chirality corresponding to each experimental Kikuchi pattern. The normalized cross-correlation coefficient r ($0 \leq |r| \leq 1$) between the experimental and simulated Kikuchi pattern of the reference structure was optimized according to (*28*), with an additional test against the inverted structure to discriminate between the enantiomorphs. The cross-correlation coefficient r_{sim} ($0 \leq |r_{sim}| \leq 1$) represents the quantified comparison between the simulated pattern of the two enantiomorphs. Sense of chirality-dependent contributions to the simulated Kikuchi pattern results in values $|r_{sim}| < 1$. The calculation of the theoretical global reference data used for the Kikuchi pattern matching was carried out using the Bloch wave approach (*17*). For each experimental pattern, two optimized correlation coefficients r_+ and r_- were obtained from the match of the simulated pattern for the structures with $P4_132$ symmetry and $P4_332$ symmetry, respectively. For the final assignment of the best-fit enantiomorph to a measured pattern and to estimate the relevance of the discrimination, the difference of the correlation coefficients $\Delta r = r_+ - r_-$, in relation to their average value $r_m = ½ (r_+ + r_-)$, is used. A large average value r_m indicates a good fit of the experimental Kikuchi pattern to the simulated data, while a simultaneous large difference $|\Delta r|$ indicates a reliable discrimination among the enantiomorphs. Reliable assignment of the absolute structure from the EBSD pattern demands substantially better match of the experimental pattern with one of the simulated patterns, with $|\Delta r| \geq 0.01$ and high-quality, experimental pattern fulfilling the condition $r_m \geq 0.5$ (*16*, *28*, *32*).

Single-crystal x-ray diffraction

X-ray diffraction datasets were collected using single crystals with cubic shape (approximate size of 30 μm), which were cut out from metallographically prepared β-Mn and Pt_2Cu_3B samples by the FIB technique using a FEI Helios G4 PFIB machine (<200 nA, 30 kV Xe beam). Cryostage equipment was used for cooling β-Mn polycrystalline material. Crystals were investigated on a Rigaku AFC-7 diffraction system equipped with a Saturn 724 CCD detector using MoKα radiation (λ = 0.71073 Å). The absorption correction of the reflection intensities was performed by a multiscan routine (*33*). All crystallographic calculations were performed with the program package WinCSD (*34*). Details of data collection and results of the structure refinement are listed in Tables 1 and 2 for Pt_2Cu_3B and β-Mn, respectively.

SUPPLEMENTARY MATERIALS

Supplementary material for this article is available at http://advances.sciencemag.org/cgi/content/full/7/20/eabg0868/DC1

REFERENCES AND NOTES

1. H. D. Flack, Chiral and achiral crystal structures. *Helv. Chim. Acta* **86**, 905–921 (2003).
2. E. Koch, W. Fischer, U. Müller, *International Tables of X-Ray Crystallography; Sixth Edition,* M. I. Aroyo, ed. (Wiley, 2016), vol. A, chap. 3.5, 826 pp.
3. S. Mühlbauer, B. Binz, F. Jonietz, C. Pfleiderer, A. Rosch, A. Neubauer, R. Georgii, P. Böni, Skyrmion lattice in a chiral magnet. *Science* **323**, 915–919 (2009).
4. E. Bauer, P. Rogl, *Noncentrosymmetric Superconductors: Strong vs Weak Electronic Correlations* (Springer, 2012).
5. A. L. Spek, Absolute structure determination: Pushing the limits. *Acta Crystallogr. B* **72**, 659–660 (2016).
6. H. D. Flack, G. Bernardinelli, The use of X-ray crystallography to determine absolute configuration. *Chirality* **20**, 681–690 (2008).
7. A. F. Peerdeman, A. J. Van Bommel, J. M. Bijvoet, Determination of absolute configuration of optically active compounds by means of X-rays. *Proc. K. Ned. Akad. Wet. Ser. B* **54**, 16–19 (1951).
8. D. Rogers, *Anomalous Scattering,* S. R. S. C. Abrahams, ed. (Munksgaard, 1975), pp. 231–250.
9. K. S. Chandrasekaran, Possibilities of 'Bijvoet differences' in non-centrosymmetric structures of elements. *Acta Crystallogr. A* **24**, 248–249 (1968).
10. R. Parthasarathy, 'Anomalous dispersion' effects in electron diffraction and their possible applications. *Acta Crystallogr.* **14**, 690–691 (1961).
11. J. M. Zuo, J. C. H. Spence, R. Hoier, Accurate structure-factor phase determination by electron diffraction in noncentrosymmetric crystals. *Phys. Rev. Lett.* **62**, 547–550 (1989).
12. J. C. H. Spence, J. M. Zuo, M. O'Keeffe, K. Marthinsen, R. Hoier, On the minimum number of beams needed to distinguish enantiomorphs in X-ray and electron diffraction. *Acta Crystallogr. A* **50**, 647–650 (1994).
13. A. J. Schwartz, M. Kumar, B. L. Adams, D. P. Fields, *Electron Backscatter Diffraction in Materials Science* (Springer, ed. 2, 2009).
14. D. Chen, J.-C. Kuo, W.-T. Wu, Effect of microscopic parameters on EBSD spatial resolution. *Ultramicroscopy* **111**, 1488–1494 (2011).
15. A. Winkelmann, G. Nolze, Chirality determination of quartz crystals using Electron Backscatter Diffraction. *Ultramicroscopy* **149**, 58–63 (2015).
16. U. Burkhardt, H. Borrmann, P. Moll, M. Schmidt, Y. Grin, A. Winkelmann, Absolute structure from scanning electron microscopy. *Sci. Rep.* **10**, 4065 (2020).
17. A. Winkelmann, C. Trager-Cowan, F. Sweeney, A. P. Day, P. Parbrook, Many-beam dynamical simulation of electron backscatter diffraction patterns. *Ultramicroscopy* **107**, 414–421 (2007).
18. A. Winkelmann, G. Nolze, Point-group sensitive orientation mapping of non-centrosymmetric crystals. *Appl. Phys. Lett.* **106**, 072101 (2015).
19. G. D. Preston, CXXV. The crystal structure of β-manganese. *London, Edinburgh, Dublin Philos. Mag. J. Sci.* **5**, 1207–1225 (1928).
20. C. B. Shoemaker, D. P. Shoemaker, T. E. Hopkins, S. Yindepit, Refinement of the structure of β-manganese and of a related phase in the Mn-Ni-Si system. *Acta Crystallogr. B* **34**, 3573–3576 (1978).
21. M. O'Keeffe, S. Andersson, Rod packings and crystal chemistry. *Acta Crystallogr. A* **33**, 914–923 (1977).
22. W. Hornfeck, P. Kuhn, Octagonal symmetry in low-discrepancy β-manganese. *Acta Crystallogr. A* **70**, 441–447 (2014).
23. T. Hama, M. Matsumura, H. Kato, H. Yamagata, Y. Kohori, T. Kohara, Y. Iwamoto, 55Mn NQR study at Mn-II sites in β-Mn metal: A possible effect of geometrical frustration. *J. Physical Soc. Japan* **73**, 2305–2312 (2004).
24. G. McIntyre, A prediction of Bijvoet intensity differences in the noncentrosymmetric structures of selenium and tellurium. *Acta Crystallogr. A* **34**, 936–939 (1978).

25. Y. Tanaka, S. P. Collins, S. W. Lovesey, M. Matsunami, T. Moriwaki, S. Shin, Determination of the absolute chirality of tellurium using resonant diffraction with circularly polarized x-rays. *J. Phys. Condes. Matter* **22**, 122201 (2010).
26. L. P. Salamakha, O. Sologub, B. Stöger, H. Michor, E. Bauer, P. F. Rogl, $(Pt_{1-x}Cu_x)_3Cu_2B$ and $Pt_9Cu_3B_5$, the first examples of copper platinum borides. Observation of superconductivity in a novel boron filled β-Mn-type compound. *J. Solid State Chem.* **229**, 303–309 (2015).
27. A. Winkelmann, G. Cios, T. Tokarski, P. Bała, Y. Grin, U. Burkhardt, Fixing left and right: Assignment of chiral elemental crystal structures using Kikuchi diffraction. arXiv:2011.14422 [cond-mat.mtrl-sci] (29 November 2020).
28. G. Nolze, R. Hielscher, A. Winkelmann, Electron backscatter diffraction beyond the mainstream. *Cryst. Res. Technol.* **52**, 1600252 (2017).
29. H. Flack, On enantiomorph-polarity estimation. *Acta Crystallogr. A* **A39**, 876–881 (1983).
30. P. J. W. Moll, Focused ion beam microstructuring of quantum matter. *Annu. Rev. Condens. Matter Phys.* **9**, 147–162 (2018).
31. K. Kaufmann, C. Zhu, A. S. Rosengarten, D. Maryanovsky, T. J. Harrington, E. Marin, K. S. Vecchio, Crystal symmetry determination in electron diffraction using machine learning. *Science* **367**, 564–568 (2020).
32. G. Naresh-Kumar, A. Vilalta-Clemente, H. Jussila, A. Winkelmann, G. Nolze, S. Vespucci, S. Nagarajan, A. J. Wilkinson, T. Trager-Cowan, Quantitative imaging of anti-phase domains by polarity sensitive orientation mapping using electron backscatter diffraction. *Sci. Rep.* **7**, 10916 (2017).
33. R. H. Blessing, An empirical correction for absorption anisotropy. *Acta Crystallogr. A* **51**, 33–38 (1995).
34. L. Akselrud, Y. Grin, WinCSD: Software package for crystallographic calculations (Version 4). *J. Appl. Cryst.* **47**, 803–805 (2014).

Acknowledgments: We thank S. Kostmann and M. Eckert of the MPI CPfS for microstructure preparation and electron microprobe analysis, respectively. **Funding:** A.W. was supported by Polish National Agency for Academic Exchange (NAWA) grant no. PPN/ULM/2019/1/00068/U/00001.
Author contributions: A.W., U.B., H.B., and Y.G. conceived the project. U.B., A.D., and G.C. prepared the samples. U.B. and G.C. measured EBSD data. H.B. performed x-ray diffraction experiments. A.W. carried out Kikuchi pattern simulation and data analysis. H.B. and Y.G. solved and refined the crystal structures. M.K. cut crystals by FIB. U.B. wrote the initial draft of the paper. Y.G., A.W., H.B., M.K., and G.C. discussed and reviewed the results and contributed to the final version of the paper. **Competing interests:** The authors declare that they have no competing interests. **Data and materials availability:** All data needed to evaluate the conclusions in the paper are present in the paper and/or the Supplementary Materials. Full sets of supplementary crystallographic data for this paper have been deposited with the joint CCDC and FIZ Karlsruhe deposition service. The data can be obtained free of charge from Inorganic Crystal Structure Database citing deposition numbers CSD 2061402-2061405.

Submitted 9 December 2020
Accepted 29 March 2021
Published 14 May 2021
10.1126/sciadv.abg0868

Citation: U. Burkhardt, A. Winkelmann, H. Borrmann, A. Dumitriu, M. König, G. Cios, Y. Grin, Assignment of enantiomorphs for the chiral allotrope β-Mn by diffraction methods. *Sci. Adv.* **7**, eabg0868 (2021).